Universiteit
Leiden
The Netherlands

Bioorthogonal labeling tools to study pathogenic intracellular bacteria

Bakkum, T.

Citation
Bakkum, T. (2021, November 17). *Bioorthogonal labeling tools to study pathogenic intracellular bacteria*. Retrieved from https://hdl.handle.net/1887/3240088

Version:	Publisher's Version
License:	Licence agreement concerning inclusion of doctoral thesis in the Institutional Repository of the University of Leiden
Downloaded from:	https://hdl.handle.net/1887/3240088

Note: To cite this publication please use the final published version (if applicable).

Chapter 6

Summary and Future Prospects

Part of this chapter was published as part of:
Floris J. van Dalen, Thomas Bakkum, Tyrza van Leeuwen, Mirjam Groenewold, Edgar Deu, Abraham Koster, Sander I. Van Kasteren, Martijn Verdoes. *Frontiers in Chemistry*, **2021**; 8(628433): 1-13.

Abstract

This chapter provides a summary of the work presented, as well as several future prospects that could be pursued, based on the techniques developed in this thesis. In the first example, both highly selective and broad-spectrum Activity Based-Probes (ABPs) are combined with Bioorthogonal Correlative Light-Electron Microscopy (B-CLEM) to study the intracellular localization of active cathepsin populations with regard to bacterial antigens, within the ultrastructure of the cell. In the second example, the localization of cathepsins is studied in combination with pathogenic and non-pathogenic bacteria, and compared to a co-infection system. In the third example, the possibility of multiple orthogonal bioorthogonal reactions is explored, for simultaneous labeling of multiple biomolecules in a single sample. Finally, the remaining challenges and limitations of the current technique are discussed, and potential improvements and alternative approaches are suggested.

6.1 Summary

In this thesis, bioorthogonal (click) chemistry is combined with in-gel fluorescence, flow cytometry, fluorescence (confocal) microscopy, super-resolution Stochastic Optical Reconstruction Microscopy (STORM), Correlative Light-Electron Microscopy (CLEM) and STORM-CLEM. Bioorthogonal chemistry as developed and applied in this thesis comprises a two-step labeling approach, in which first a bioorthogonal group or 'click handle' is incorporated into a biological system of interest by exploiting the organism's natural metabolism (also known as metabolic labeling), followed by a biocompatible ligation reaction or 'click reaction' to attach a fluorophore for detection. In this way, the initial label exerts minimal interference on the biochemistry and biology of the targeted organism, while it can be detected by exploiting its intrinsic capability to selectively attach a fluorophore at the desired time. For many purposes, the fluorophore can be attached at the end of a biological time course, following chemical fixation to preserve the (sub)cellular distribution of biological components like proteins, carbohydrates and fatty acids. Combining this convenient labeling strategy with the appropriate analysis technique can provide useful information about the cellular content (flow cytometry), localization (confocal microscopy), subcellular distribution (CLEM) and even single-molecule distribution within the ultrastructure of the cell (STORM-CLEM).

In **chapter 1** a general introduction about bioorthogonal chemistry and its application for fluorescent analyses and imaging is presented. The general principles of bioorthogonal chemistry and metabolic labeling are introduced, and applications of bioorthogonal metabolic labeling to bacteria. Finally, the broad compatibility of bioorthogonal chemistry is illustrated by highlighting its potential application to the various analysis methods described above.

In **chapter 2** recent advancements in the field of metabolic labeling for imaging of intracellular pathogenic bacteria are reviewed. Recent results in metabolic labeling of the bacterial proteome, peptidoglycan and the mycomembrane of corynebacteria are described, and compared to another widely used chemical labeling methodology: Activity-Based Protein Profiling (ABPP). The application of both labeling approaches in imaging techniques is discussed, within the context of intracellular pathogenic bacteria.

Chapter 3 describes that terminal alkynes and azides – two of the most widely applied bioorthogonal functionalities in metabolic labeling – are resistant to even the harshest of biochemical environments found in phagocytic cells of the immune system (dendritic cells and macrophages), while the widely used strained alkynes

BCN and DBCO quickly degrade under these conditions. In this chapter, flow cytometry was exploited to measure the fluorescence of click handle-modified beads, after attaching a fluorophore to each of the click handles by copper-catalyzed or strain-promoted Huisgen-type cycloaddition reactions (ccHc and spHc, respectively). This allowed the quantification of click handle stability, since degradation of these handles reduced the number of fluorophores per bead, thus resulting in a lower fluorescent signal. Terminal alkynes proved ideal for labeling of biological systems such as bacteria for two reasons: 1) terminal alkynes were found to be resistant to the lysosomal compartments of the phagocytes (<6% degraded) and 2) azide-containing fluorophores showed significantly lower background fluorescence compared to the alkyne-containing fluorophore, in the inverse labeling strategy.

In **chapter 4** bioorthogonal labeling is used to visualize the facultative intracellular pathogen *Salmonella enterica* serovar Typhimurium (*Stm*) within the host phagocyte, through incorporation of bioorthogonal amino acids into the proteome or cell wall of *Stm*. Optimization of label incorporation was achieved using in-gel fluorescence analysis, flow cytometry and STORM. Incorporation of either L-azidohomoalanine (Aha) or L-homopropargylglycine (Hpg) into the proteome was successful with negligible effect on bacterial viability but the alkyne-containing Hpg was preferred due to the lower background level of the azide-containing fluorophore, as discovered in chapter 3. Incorporation of D-propargylglycine (alkDala) into the peptidoglycan of the cell wall of *Stm* was also successful but proved inferior to Hpg in terms of labeling efficiency. The Hpg-labeled *Stm* were subsequently used to study their infection of dendritic cells, using flow cytometry and STORM-CLEM. Within this context, STORM-CLEM allowed for a >10-fold resolution improvement compared to confocal-CLEM, as well as providing single-molecule detection, improved signal-to-noise ratio and crisper images with more details. Some small labeled structures were detected outside of the bacterial structure, which may represent secreted *Stm* proteins, although this remains to be confirmed.

In **chapter 5** the bioorthogonal labeling strategy, described in chapter 4, is translated to a more dangerous and clinically relevant facultative intracellular pathogen, *Mycobacterium tuberculosis* (*Mtb*) which is the causative agent of tuberculosis (TB). All analysis techniques had to be customized for *Mtb* due to its excessively thick and complex mycobacterial cell wall. In-gel fluorescence, flow cytometry, on-section confocal microscopy and CLEM were used to optimize the incorporation of bioorthogonal amino acids into the bacterial proteome and cell

wall of *Mtb*. Successful triple labeling of *Mtb* was achieved by combining DsRed fluorescent protein expression with Aha-labeling of the bacterial proteins and alkDala-labeling of the cell wall.

Using these techniques, new information about the complex intracellular behavior of *Mtb* in macrophages was obtained. Most importantly, the effect of three first-line anti-tuberculosis drugs (rifampicin, isoniazid and ethambutol) on intracellular distribution and shape of the bacteria was quantified using B-CLEM. Moreover, the effect of these drugs on label retention (Aha, alkDala and DsRed) was quantified using flow cytometry. The three drugs combined had the strongest effect on intracellular distribution, relocating almost every bacterium to a large/spacious vacuole. Surprisingly, this triple drug combination did not have the strongest effect on label retention but instead an intermediate effect, suggesting some mutual drug-drug interference may occur.

6.2 Future prospects

Whereas the bioorthogonal CLEM (B-CLEM) method presented in this thesis has proven to be of great value to the study of pathogenic intracellular bacteria such as *Mtb*, it should be of equal value in addressing various other biological questions. For example, the degradation and further processing of non-pathogenic bacteria towards antigen presentation could be studied in more detail. Alternatively, the differences between pathogenic and non-pathogenic bacteria could be investigated, as well as the triggers that cause a non-pathogenic strain to become pathogenic. Even for *Mtb*, many questions still remain that could be answered with B-CLEM and related techniques such as bioorthogonal STORM-CLEM, flow cytometry and proteomics. Moreover, the B-CLEM approach could still be improved and expanded in several ways. Whereas B-CLEM has thus far mostly been used in combination with bioorthogonal amino acids – to study the fate of intracellular bacteria – it may also be combined with different bioorthogonal probes, such as metabolic labels for non-protein biomolecules or selective enzyme probes. Additionally, since the B-CLEM approach is based on the Tokuyasu method for cryo-sectioning, it should also be compatible with direct fluorescent probes (e.g. fluorescent enzyme probes or fixable organelle trackers), as well as immunofluorescence and immunogold labeling. This would expand the scope of potential targets and potentially increase the number of targets that can be studied simultaneously in a single sample. Another way to increase the number of targets would be to use multiple click ligation reactions that can be performed in a single sample without cross-reacting, so-called mutually orthogonal bioorthogonal

reactions. A first step towards this goal has already been illustrated in **chapter 5** where two metabolic labels, containing either an azide or an alkyne, could be reacted selectively to different fluorophores, using two sequential ccHc reactions.

6.2.1 Application of a Highly Selective Cathepsin S Two-Step Activity-Based Probe in B-CLEM

One way in which the B-CLEM approach could be improved would be to use a highly selective Activity-Based Probe (ABP) to specifically target an enzyme of interest. Cathepsin S (Cat S) is a lysosomal cysteine protease highly expressed in immune cells such as dendritic cells, B cells and macrophages.[1,2] Its functions include extracellular matrix breakdown and cleavage of cell adhesion molecules to facilitate immune cell motility, as well as cleavage of the invariant chain during maturation of MHC II.[3–9] Cat S is a major factor in MHC II-mediated antigen presentation and there is compelling (though not yet conclusive) evidence that it also contributes to MCH I-mediated cross-presentation.[6–8] The identification of these diverse specific functions has brought the challenge of delineating Cat S activity with great spatial precision, relative to related enzymes and substrates.

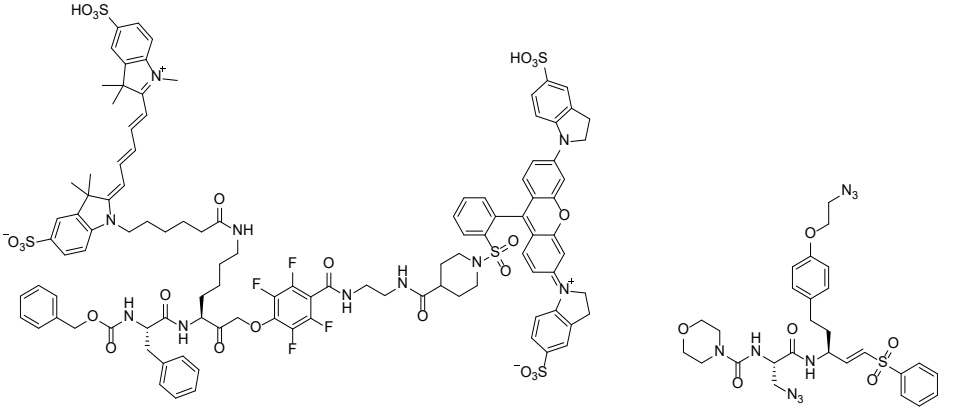

Figure 1. Activity-Based Probes selective for cysteine cathepsins (BMV109)[10] or cathepsin S only (FJD239)[11].

When applying a potent and highly selective azide-containing ABP for Cat S (FJD239; **Figure 1**), confocal microscopy and B-CLEM can provide valuable information on the subcellular localization of Cat S. The broad compatibility of this technique allows for simultaneous identification of related cysteine cathepsins using a broad-spectrum ABP (BMV109), as well as a relevant bioorthogonally-labeled antigen (Hpg-*E. coli*) during degradation (**Figure 2**).

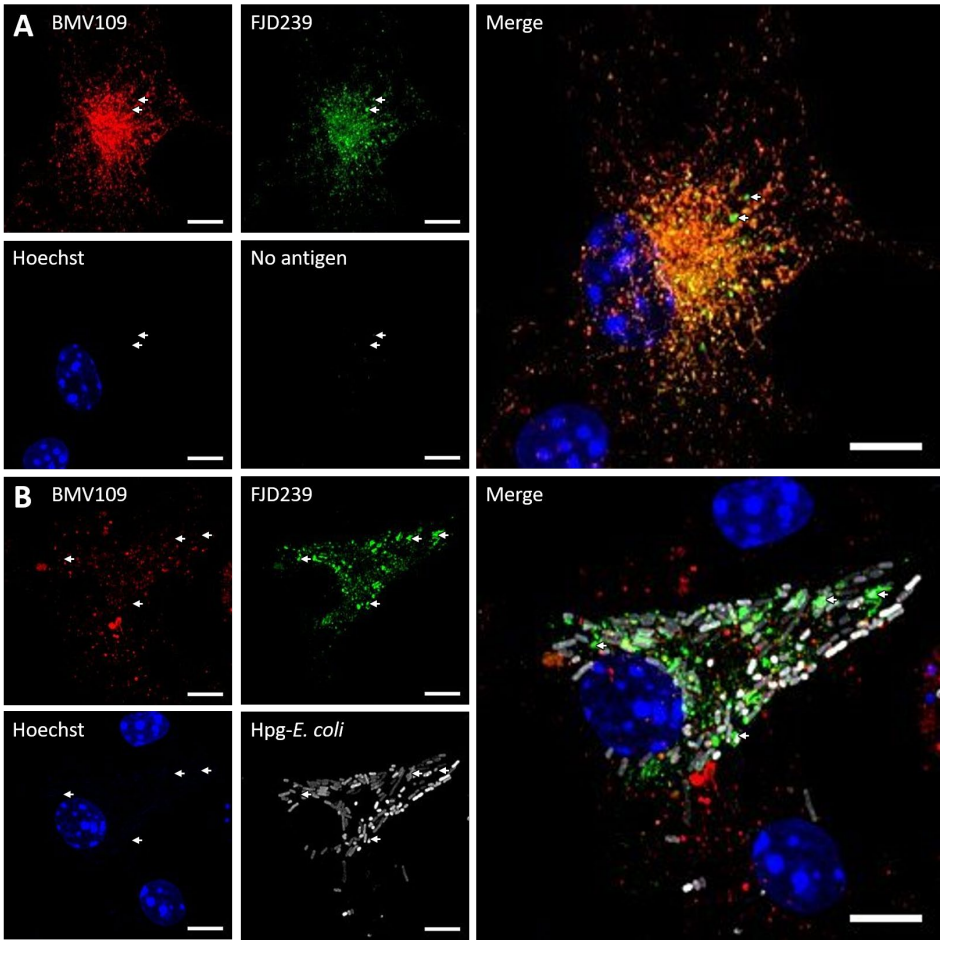

Figure 2. Localization of Cat S, studied by confocal microscopy. (**A**) Naïve BMDCs (at time point 0) were treated with FJD239 (green) for one hour and BMV109 (red) for one hour, and FJD239 was visualized through ccHC. (**B**) BMDCs were pulsed with Hpg-labeled E. coli (white) for 45 minutes, followed by treatment with FJD239 (green) for one hour and BMV109 (red) for one hour. Hpg-E. coli and FJD239 were visualized by dual ccHc with AFDye555-azide and AF488-alkyne. DNA was counterstained with Hoechst for reference. Vesicles containing only Cat S are annotated with white arrows. Scale bar represents 5 µm.

Although colocalization of bacterial antigen with cathepsins was prevalent, a high variance in cathepsin activity between cells was observed (**Figure 2**). This may follow from the fact that the GM-CSF-generated BMDCs used here, form a highly heterogeneous population of monocytic cells.[12] It was also noted that occasionally, intact bacteria could still be observed at three hours post-infection. While most vesicles labelled positive for both Cat S activity and the broad-spectrum cathepsin probe, some vesicles can be observed that exclusively contain Cat S activity without detectable activity of the other cathepsins (**Figure 2, arrows**), which is in line with a previous observation by Bender and co-workers.[10] The exact function and nature of these vesicles remain elusive but would be interesting to study further.

Since the B-CLEM method is compatible with immunogold labeling, additional proteins of interest (e.g., MHC II or LAMP1) can be identified, thereby overcoming the limited number of fluorescent channels (normally 4). Ultimately, this allows for the localization of Cat S (green) relative to other cathepsins (red), antigen (magenta) and LAMP1 (15 nm gold; **Figure 3**) or MHC II (15 nm gold; **Figure 4**). The number of labeled molecules of interest in one image can be increased even more by combining various sizes of gold particles (5, 10 & 15 nm).[13] Alternatively, the number of fluorescent channels can be increased by adding an additional near-infrared laser, or using tandem dyes.[14]

The first example clearly illustrates the presence of LAMP1 on bacteria-containing phagosomes (**Figure 3**, arrow 1/2), as well as on vesicles containing both Cat S and other lysosomal cathepsins (**Figure 3**, arrow 3). Although complete colocalization of Hpg-*E. coli* with cathepsins was not observed in this example, large cathepsin-containing vesicles (**Figure 3**, arrow 3/4) are in close proximity of the phagosomes and may be in a process of fusion or exchange of contents.[15,16] One of the bacterial profiles is small and irregular in shape (**Figure 3**, arrow 2), suggesting partial degradation has already occurred (for more information see **chapter 5**). Although no quantification can be performed on this example alone, most of the detected Cat S activity appear in close proximity to this partially-degraded bacterium. Indeed, Cat S was shown to be actively involved with antigen presentation[6], amongst various other activities.

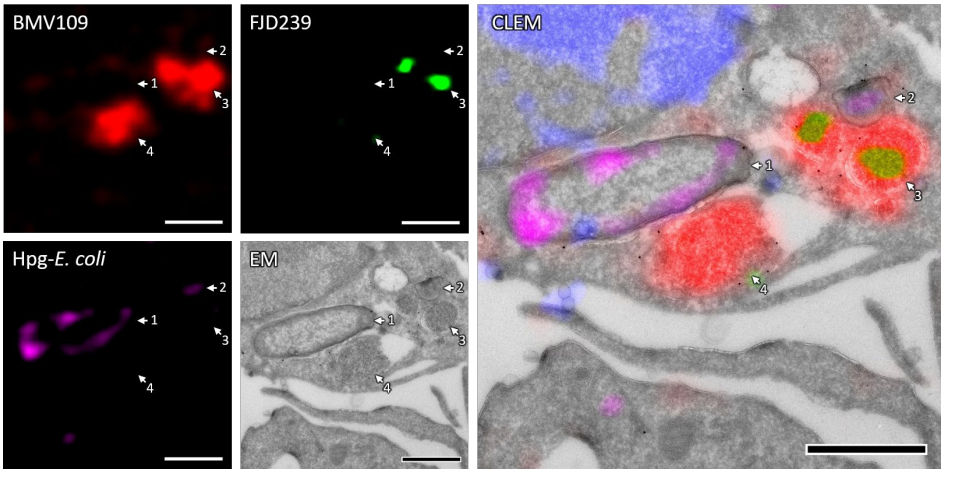

Figure 3. The involvement of Cat S in bacterial degradation, studied by B-CLEM. BMDCs were pulsed with Hpg-E. coli (magenta) for 45 minutes, followed by treatment with FJD239 (green) for one hour and BMV109 (red) for one hour. Cryo-sectioning was followed by on-section dual ccHc with AFDye555-azide and AF488-alkyne, and LAMP1 was visualized with 15 nm immunogold labelling (black dots). The nuclei were stained with DAPI (blue) and the confocal and TEM images were correlated. Scale bar represents 1 µm.

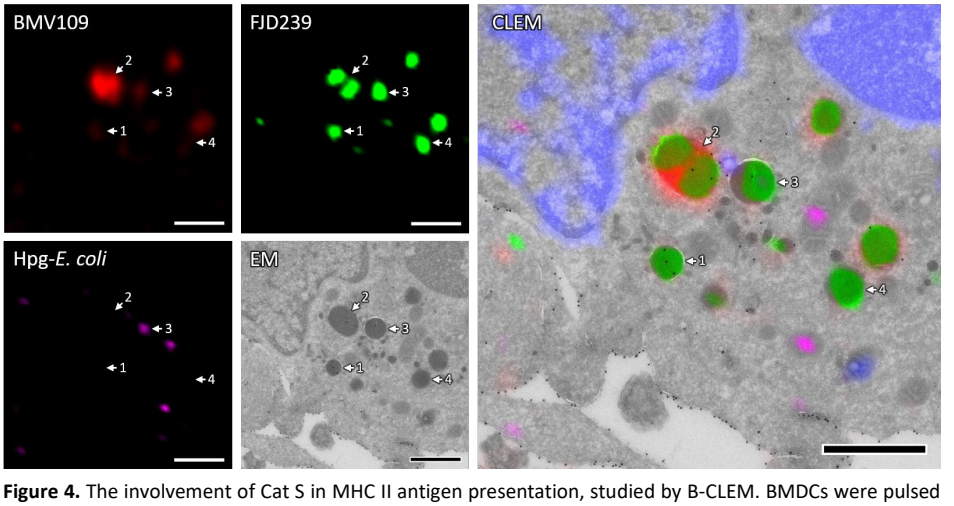

Figure 4. The involvement of Cat S in MHC II antigen presentation, studied by B-CLEM. BMDCs were pulsed with Hpg-E. coli (magenta) for 45 minutes, followed by treatment with FJD239 (green) for one hour and BMV109 (red) for one hour. Cryo-sectioning was followed by on-section dual ccHc with AFDye555-azide and AF488-alkyne, and MHC II was visualized with 15 nm immunogold labelling (black dots). The nuclei were stained with DAPI (blue) and the confocal and TEM images were correlated. Scale bar represents 1 µm.

The second example shows the presence of MHC II both on the plasma membrane and inside several vesicles. These MHC II-positive vesicles appear to contain either (almost) exclusively Cat S (**Figure 4**, arrow 1) or a combination of Cat S and other lysosomal cathepsins (**Figure 4**, arrow 2). A vesicle that apparently contains both Cat S and bacterial digest was observed as well (**Figure 4**, arrow 3), suggesting Cat S may indeed be involved in antigen processing in this example. Another vesicle can be observed, apparently containing exclusively Cat S but no MHC II (**Figure 4**, arrow 4). The presence of MHC II on Cat S-positive vesicles clearly illustrates a role for MHC II in antigen presentation, consistent with literature.[6] It would be interesting to study the localization of Cat S with respect to MHC I, to potentially confirm that Cat S is involved in the production of antigenic peptides for cross-presentation.[7]

Although no definitive biological conclusions can be drawn from this pilot study, it clearly illustrates the potential of four color, dual bio-orthogonal fluorescence imaging in combination with CLEM and immunogold labelling. Together, this exemplifies the great applicability of FJD239 in fluorescence microscopy and state-of-the-art dual B-CLEM.

6.2.2 Studying the role of cathepsins in bacterial degradation and immune evasion using CLEM

B-CLEM has previously been used to study degradation of *E. coli* in dendritic cells, which showed colocalization of small Aha-positive foci, representing partially degraded bacteria, with lysosomal associated membrane protein 1 (LAMP1)-positive compartments of the host cell.[17] This implied that the Aha-labeled *E. coli* were degraded inside host cell lysosomes, which is in line with existing knowledge of the bacterial degradation pathway.[18] However, this only confirms the initial uptake and degradation of *E. coli* until the degradation products reach the late phagosomes/phagolysosomes but do not clarify the subsequent processing towards antigen presentation. Several specialized lysosomal hydrolases, including multiple cathepsins, are involved in the processing of large foreign antigens (such as bacteria) into small antigenic peptides that can be presented on Major Histocompatibility Complex (MHC) II via the classical pathway or on MHC I via so-called antigen cross-presentation.[19]

When applying a broad-spectrum ABP for cysteine cathepsins (BMV109; **Figure 1**), confocal microscopy and CLEM can provide valuable information on the subcellular localization of *E. coli*, with respect to enzymatically active cathepsins. Although fluorescent proteins can be inactivated during bacterial degradation, GFP was

found to remain surprisingly fluorescent and can therefore be used as a practical first step in studying the degradation process by CLEM. However, bioorthogonally-labeled *E. coli* will be more suitable to study antigen processing in more detail, since it remains detectable for longer periods of time.[17]

Confocal microscopy of dendritic cells, shortly after phagocytosis of the bacteria did not yet show colocalization of the lysosomal cathepsins with GFP-*E. coli* (**Figure 5**). However, in some cases large cathepsin-containing vesicles were found in close proximity to the bacterium, suggesting that fusion between phagosome and lysosomes may follow (**Figure 5**, arrows).

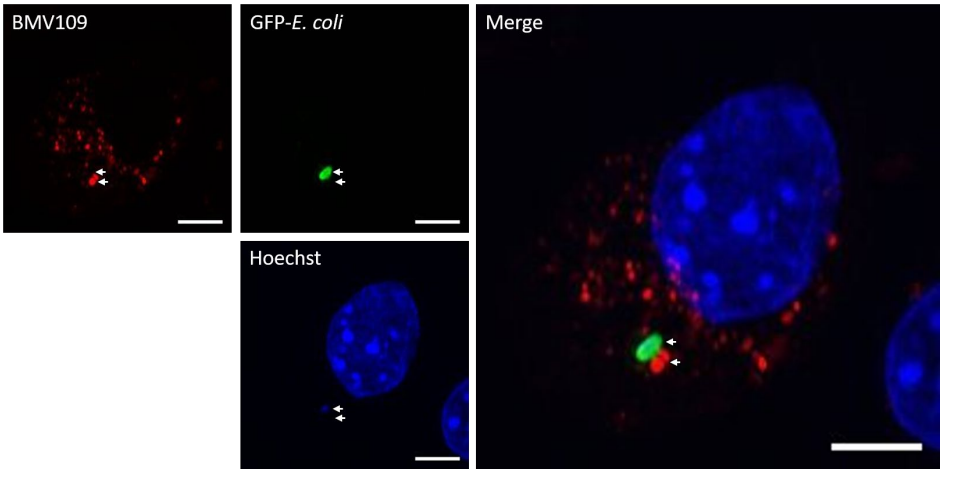

Figure 5. Localization of E. coli relative to active cathepsins, studied by confocal microscopy. DC2.4 dendritic cells were pulsed with GFP-expressing E. coli (green) for 45 minutes, followed by treatment with BMV109 (red) for one hour. DNA was counterstained with Hoechst for reference. Top arrow indicates an E. coli bacterium, bottom arrow indicates large cathepsin-containing vesicles. Scale bar represents 5 µm.

CLEM confirmed that GFP-expressing *E. coli* (green) do not yet colocalize with active cathepsins (red) shortly after uptake (**Figure 6**) but show considerable colocalization after one hour chase in dendritic cells (**Figure 7**). As observed above, the cathepsin-containing vesicles are in close proximity to the bacteria-containing phagosomes but did not yet fuse for the earliest time point (**Figure 6**, arrows). After one hour chase, a large compartment was observed that contains a clear GFP-positive bacterial structure, surrounded by a large BMV109-positive vacuole (**Figure 7**, arrow). This compartment can be considered a classical phagolysosome due to the co-occurrence of a bacterium and the active lysosomal cathepsins.[15] Indeed,

some of the large bacterial antigen appears to be processed into smaller pieces that lack a recognizable structure after three hours (**Figure 8**, arrow). This smaller GFP-positive antigen seems to be localized in a multi-vesicular compartment, which is in accordance with literature, as it was found that MHC II and its associated antigens are often found in multivesicular bodies.[20,21]

Additional research using B-CLEM, STORM-CLEM (see **chapter 4**) and further quantification (see **chapter 5**) could shine a light on the antigen processing pathway and help to further elucidate the process of antigen (cross-)presentation. Indeed bioorthogonal model antigens have recently been used to study the effect of posttranslational modifications on antigen processing and presentation[22], whereas bioorthogonal antigens have also been used to obtain chemical control over T cell activation.[23,24] Ideally, the entire pathway from bacterial or viral uptake until antigen (cross-)presentation can be studied using the techniques described in this thesis, in combination with other techniques such as proteomics[25], to further elucidate this process and open new doors for therapeutic intervention.

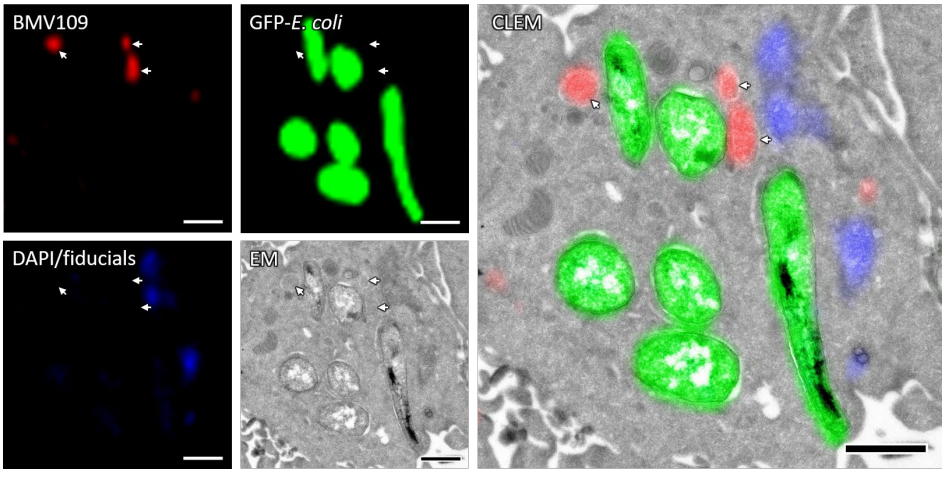

Figure 6. The involvement of cathepsins in bacterial degradation directly after uptake, studied by CLEM. D1 cells were pulsed with GFP-expressing E. coli (green) for 45 minutes, followed by treatment with BMV109 (red) for one hour. Cryo-sectioning was performed according to the Tokuyasu method. The nuclei were stained with DAPI (blue) and the confocal and TEM images were correlated. Arrows indicate BMV109-positive compartments. Scale bar represents 1 µm.

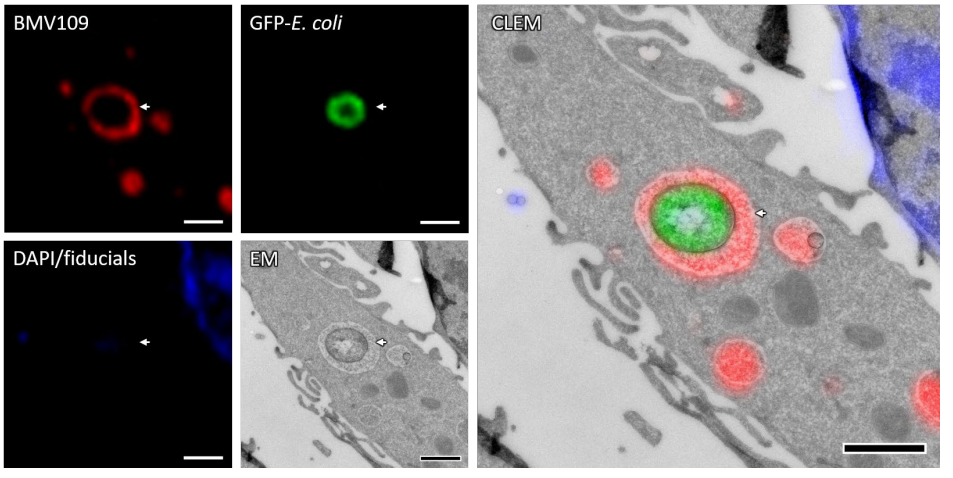

Figure 7. The involvement of cathepsins in bacterial degradation one hour post-uptake, studied by CLEM. D1 cells were pulsed with GFP-expressing E. coli (green) for 45 minutes and chased for one hour, followed by treatment with BMV109 (red) for one hour. Cryo-sectioning was performed according to the Tokuyasu method. The nuclei were stained with DAPI (blue) and the confocal and TEM images were correlated. Arrow indicates a large GFP-positive and BMV109-positive compartment. Scale bar represents 1 µm.

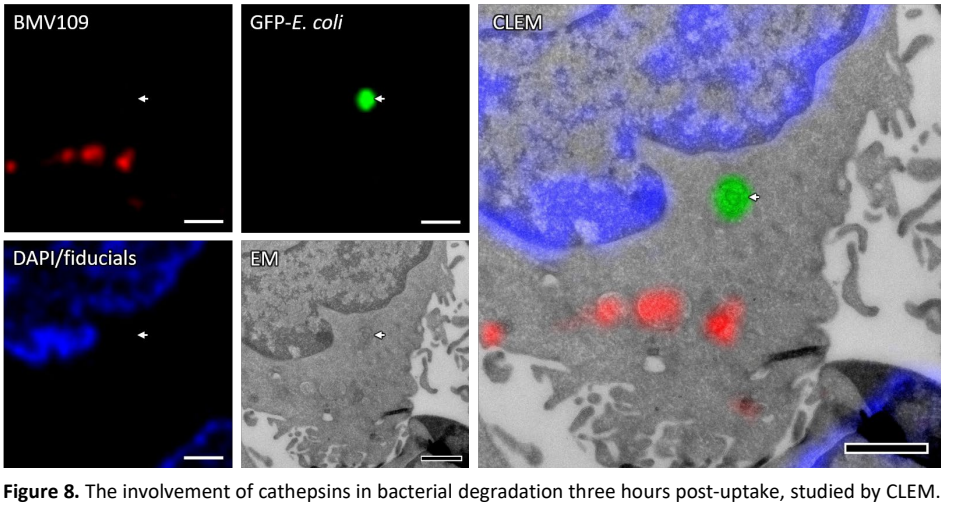

Figure 8. The involvement of cathepsins in bacterial degradation three hours post-uptake, studied by CLEM. D1 cells were pulsed with GFP-expressing E. coli (green) for 45 minutes and chased for three hours, followed by treatment with BMV109 (red) for one hour. Cryo-sectioning was performed according to the Tokuyasu method. The nuclei were stained with DAPI (blue) and the confocal and TEM images were correlated. Arrow indicates a GFP-positive multivesicular compartment. Scale bar represents 1 µm.

Contrary to the non-pathogenic *E. coli*, intracellular pathogenic bacteria have evolved many ways to evade the host immune response, thereby allowing them to survive and often even proliferate inside host (immune) cells[26]. One of the survival strategies employed by *Stm* is to inhibit fusion of the *Salmonella*-containing vacuole (SCV) with lysosomes through several (secreted) effector proteins[27,28], effectively avoiding exposure to acidic pH, antimicrobial peptides and hydrolytic enzymes[29,30]. Indeed, when DsRed-expressing *Stm* was studied by CLEM, colocalization of *Stm* with lysosomes (judged by BMV109 fluorescence) was not detected (**Figure 9**), although close encounters were observed (**Figure 10, arrow**).

Interestingly, when allowing both *E. coli* and *Stm* to infect dendritic cells simultaneously, colocalization of *Stm* with cathepsins appears to be more prevalent in cells containing both bacterial species (**Figure 11, top arrow**), suggesting an immunostimulatory effect may be elicited by the presence of *E. coli*. Cells containing only *Stm* are less likely to show colocalization of this bacterium with cathepsins (**Figure 12**). This effect must be quantified and further studied to confirm (or reject) this observation but it is interesting to speculate that immune-modulatory secreted proteins from *Stm*[31] may protect the bystander *E. coli* in this context.

There is a clear difference between the *Stm*-containing vacuole, which spaciously surrounds the bacterium, and the *E. coli*-containing vacuole that is tightly wrapped around the bacterium (**Figure 11**). This allows for reliable identification of the bacterial species, even when the fluorescent protein loses fluorescence (**Figure 12, top arrow**), either due to degradation or loss of expression. Interestingly, in the small dataset presented here (n≈500 bacteria), *Stm* seems to lose DsRed fluorescence before structural integrity, while *E. coli* appears to lose its structural integrity before GFP fluorescence. Loss of DsRed fluorescence by Stm may either represent degradation (**Figure 11, arrow**) or loss of its expression plasmid and subsequent proliferation, resulting in fluorescent protein dilution. Loss of structure (as the result of degradation) by *E. coli* is often accompanied by the presence of small vesicles surrounding or inside the bacterial structure, as well as colocalization with cathepsins, suggesting phagolysosomal degradation is occurring (**Figure 13**).

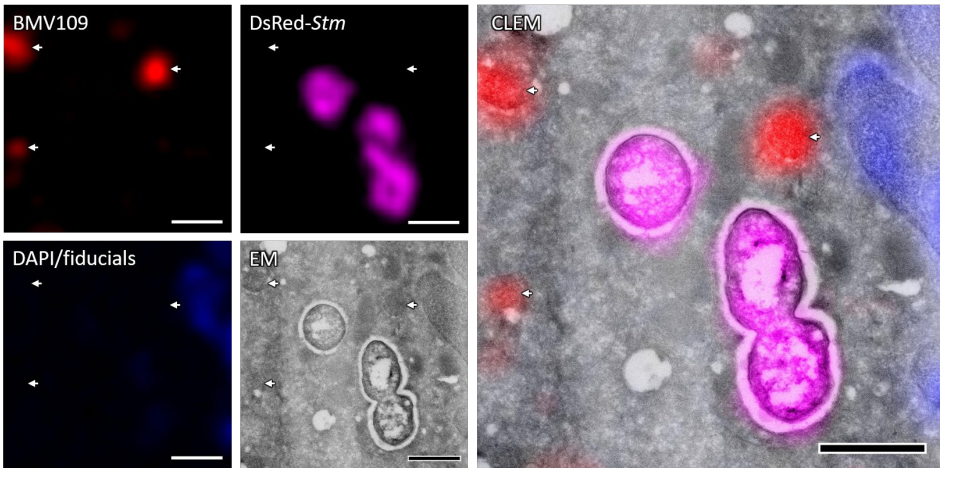

Figure 9. The involvement of cathepsins in Stm immune evasion, studied by CLEM (example 1). D1 cells were pulsed with DsRed-expressing Stm (magenta) for 45 minutes and chased for one hour, followed by treatment with BMV109 (red) for one hour. Cryo-sectioning was performed according to the Tokuyasu method. The nuclei were stained with DAPI (blue) and the confocal and TEM images were correlated. Arrows indicate BMV109-positive compartments. Scale bar represents 1 µm.

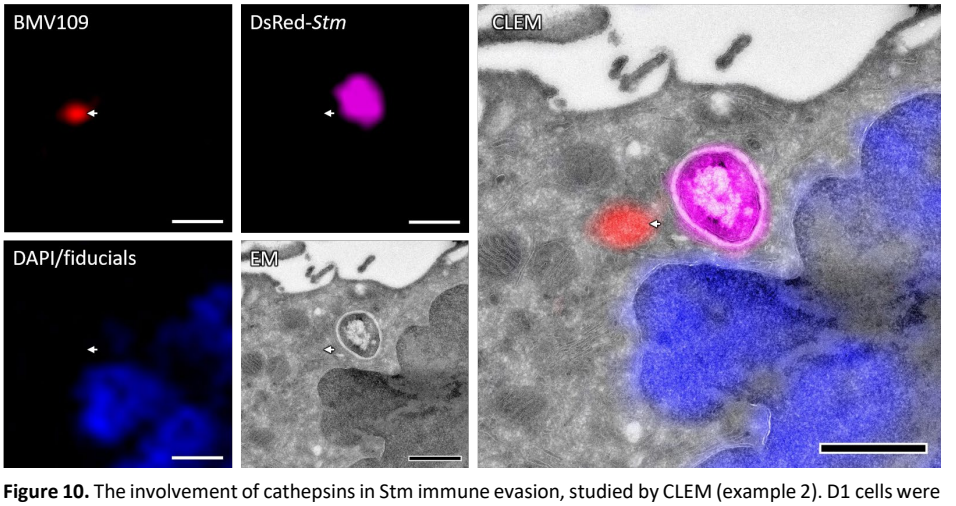

Figure 10. The involvement of cathepsins in Stm immune evasion, studied by CLEM (example 2). D1 cells were pulsed with DsRed-expressing Stm (magenta) for 45 minutes and chased for one hour, followed by treatment with BMV109 (red) for one hour. Cryo-sectioning was performed according to the Tokuyasu method. The nuclei were stained with DAPI (blue) and the confocal and TEM images were correlated. Arrow indicates a BMV109-positive compartment. Scale bar represents 1 µm.

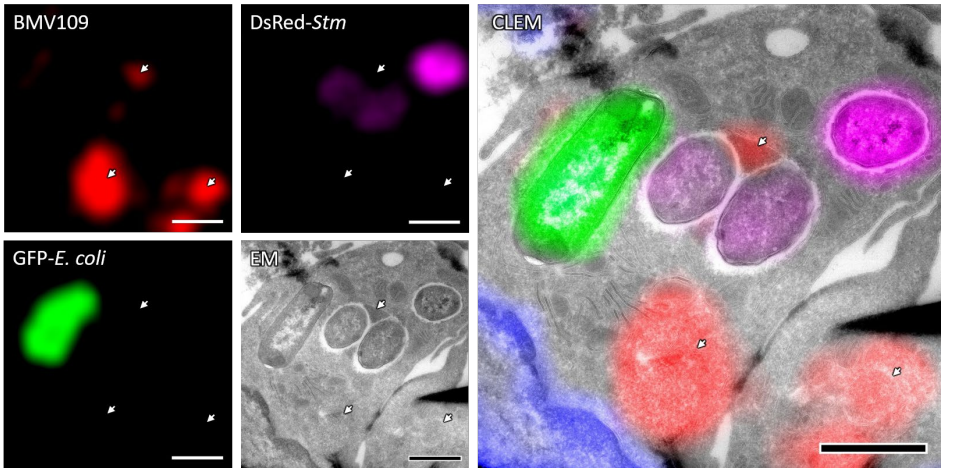

Figure 11. The involvement of cathepsins in bacterial degradation in a dual-infection system with E. coli and Stm, studied by CLEM (example 1). D1 cells were pulsed with GFP-expressing E. coli (green) and DsRed-expressing Stm (magenta) simultaneously for 45 minutes and chased for one hour, followed by treatment with BMV109 (red) for one hour. Cryo-sectioning was performed according to the Tokuyasu method. The nuclei were stained with DAPI (blue) and the confocal and TEM images were correlated. Arrows indicate BMV109-positive compartments. Scale bar represents 1 µm.

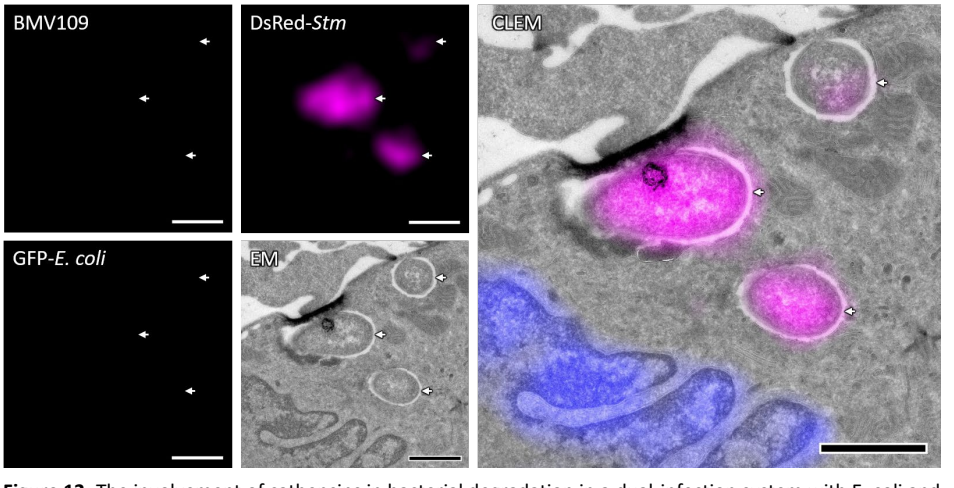

Figure 12. The involvement of cathepsins in bacterial degradation in a dual-infection system with E. coli and Stm, studied by CLEM (example 2). D1 cells were pulsed with GFP-expressing E. coli (green) and DsRed-expressing Stm (magenta) simultaneously for 45 minutes and chased for one hour, followed by treatment with BMV109 (red) for one hour. Cryo-sectioning was performed according to the Tokuyasu method. The nuclei were stained with DAPI (blue) and the confocal and TEM images were correlated. Arrows indicate Stm-containing vacuoles. Scale bar represents 1 µm.

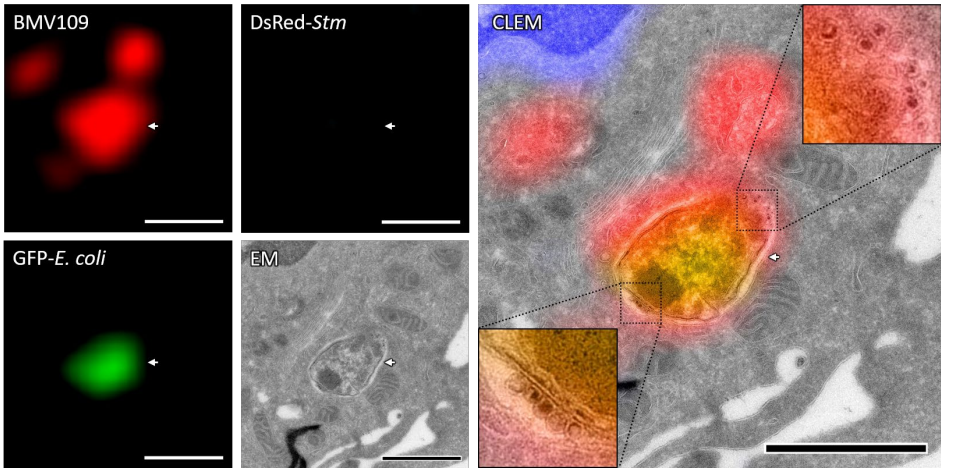

Figure 13. The involvement of cathepsins in bacterial degradation in a dual-infection system with E. coli and Stm, studied by CLEM (example 3). D1 cells were pulsed with GFP-expressing E. coli (green) and DsRed-expressing Stm (magenta) simultaneously for 45 minutes and chased for one hour, followed by treatment with BMV109 (red) for one hour. Cryo-sectioning was performed according to the Tokuyasu method. The nuclei were stained with DAPI (blue) and the confocal and TEM images were correlated. Arrow indicates a BMV109-positive, E. coli-containing compartment. Boxes show zoom-ins of the indicated regions. Scale bar represents 1 µm.

Once again, additional research using B-CLEM, STORM-CLEM and further quantification could help to further elucidate the immune-evading strategies of *Stm*, as well as provide information on the effect of co-infection by multiple pathogenic and non-pathogenic bacteria. Moreover, it would be interesting to use B-CLEM to study pathogenic *E. coli* variants such as the enteropathogenic *E. coli* (EPEC), uropathogenic *E. coli* (UPEC) or meningitis-associated *E. coli* (MNEC), which cause enteric/diarrheal disease, urinary tract infections (UTIs) and sepsis/meningitis, respectively.[32]

6.2.3 Triple orthogonal bioorthogonal reactions for further expansion of the B-CLEM method

Using multiple bioorthogonal reactions simultaneously to selectively label more than one biomolecule in a single experiment, has been a topic of great interest to chemical biologists, ever since the discovery of the first bioorthogonal reaction.[33,34] Several mutually orthogonal bioorthogonal reactions have been discovered to date[35] and have been applied to label up to three different targets in a single sample.[36–41] In this thesis, it was found that even the copper-catalyzed azide-alkyne ligation can be performed in conjunction with the inversed alkyne-azide ligation in a single microscopy sample, as long as the bioorthogonal labels are incorporated

into different parts of the cell, and the reactions are performed sequentially with intermediate washing (**chapter 5**). Given the fact that several bioorthogonal reactions are mutually orthogonal (**Figure 14**), this theoretically allows for at least three different bioorthogonal ligations in one microscopy sample.

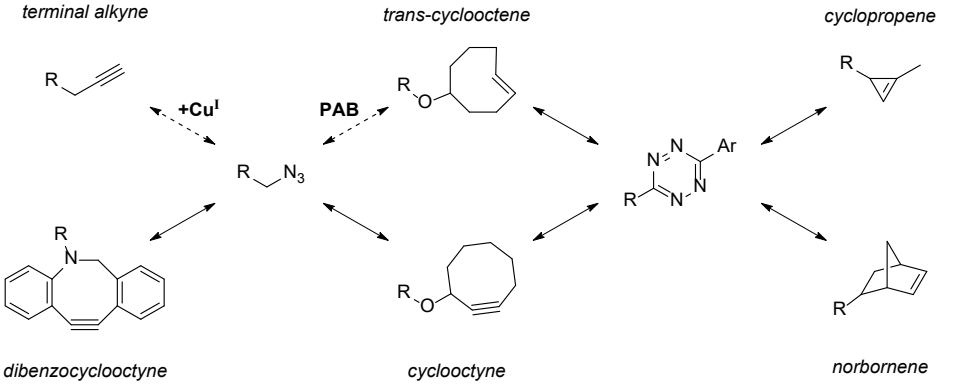

Figure 14. Reactivity profile of the most commonly used bioorthogonal groups. Arrows indicate reactivity between indicated groups. Dashed arrow indicates reactivity occurs exclusively under special conditions; $+Cu^{I}$ = copper(I)-catalyzed conditions are required for reaction to occur[42], PAB = para-azidobenzyl is required for this reaction to occur[43].

A potential triple orthogonal bioorthogonal ligation (triple click) strategy could be a combination of alkyne, azide and cyclopropene metabolic labels, which are mutually unreactive in the absence of copper(I). The corresponding reporter moieties (e.g. fluorophores) can be chosen with some flexibility, depending on the nature of the sample and the analysis method. An alkyne label can only react with an azide-reporter and exclusively under copper-catalyzed conditions. An azide label can be ligated either to an alkyne-reporter under copper-catalyzed conditions or to a cyclooctyne-reporter under copper-free conditions. Since cyclooctynes react with tetrazines as well, the bulky dibenzocyclooctyne (DBCO) is the preferred reaction partner for azides, as it is sterically hindered in its reaction with aryltetrazines.[35] Strained cycloalkenes readily react with tetrazines but the rate of reaction heavily depends on the actual structure of both the cycloalkene and the tetrazine.[44–46] When prioritizing the small size of bioorthogonal label (as for the alkyne and azide groups) the cyclopropene is the obvious choice. The corresponding reporter must then contain a tetrazine but the exact structure (R and Ar groups) remains open for optimization.

When applying this triple click strategy to the metabolic labelling and imaging strategy presented in this thesis, a combination of the alkyne-containing nucleoside 5-ethynyl-2'-deoxyuridine (EdU), the azide-containing sugar 1,3,4,6-tetra-*O*-acetyl-*N*-azidoacetylmannosamine (Ac4ManNAz) and the cyclopropene-containing fatty acid sterculic acid (StA) can be used. To confirm the viability of this approach, cells were incubated with the three metabolic labels simultaneously for two hours, followed by fixation with PFA and permeabilization with Triton-X100 with intermediate washing. A sequential triple click approach was chosen, with intermediate washing steps to minimize potential cross-reactivity or interference. StA was first reacted to 5 µM AFDye 488-tetrazine in PBS for one hour, followed by a washing step with PBS to remove excess dye. EdU was next reacted to 5 µM AFDye 647-azide under ccHc conditions, followed by a washing step with PBS to remove excess dye. Finally, Ac4ManNAz was reacted to 5 µM AFDye 555-alkyne under ccHc conditions, followed by a washing step with PBS to remove excess dye and a 30 minute wash with 1% BSA in PBS to remove any non-specifically bound dye. Indeed, the three click reactions were found to be mutually orthogonal, succeeding in selectively labelling StA, Ac4ManNAz and EdU (**Figure 15A**) without any detectable background staining (**Figure 15B**).

It would be interesting to combine this triple click approach with CLEM as it creates the possibility to study three metabolic bioorthogonal labels simultaneously, at the subcellular level. This could for example allow the study of three bacterial components (e.g., proteins, peptidoglycan and lipids) simultaneously and observe how these components are processed by the host immune cell after degradation of the bacterium. Alternatively, this approach could be reversed to study the uptake of host components by an intracellular pathogenic bacterium, in order to understand which nutrients are taken up by the pathogen under different conditions, *in situ*.

Theoretically, a fourth orthogonal group could be added for a quadruple click strategy but when considering only the bioorthogonal groups discussed here, selectivity will have to be obtained through the difference in reaction rate and/or sterics.[46] Hypothetically, kinetic selectivity could be obtained between the fast trans-cyclooctene (TCO) and the slow norbornene group or even an unstrained vinyl group, which has been shown to react with tetrazines, albeit slowly.[47] When considering steric factors, selectivity can be obtained between a TCO and a cyclopropene group, when using two different tetrazines containing either small or bulky side groups.[46] Alternatively, a fourth (and potentially even fifth) orthogonal group may potentially be found in the ever expanding collection of novel

bioorthogonal chemistries.[41,48,49] Since pure orthogonality in reactivity is difficult to obtain, special conditions may be required to obtain a fourth fully orthogonal group such as photoinduction.[50] It remains to be experimentally confirmed if these bioorthogonal labeling and ligation strategies can indeed be applied to a single sample, without cross-reactivity.

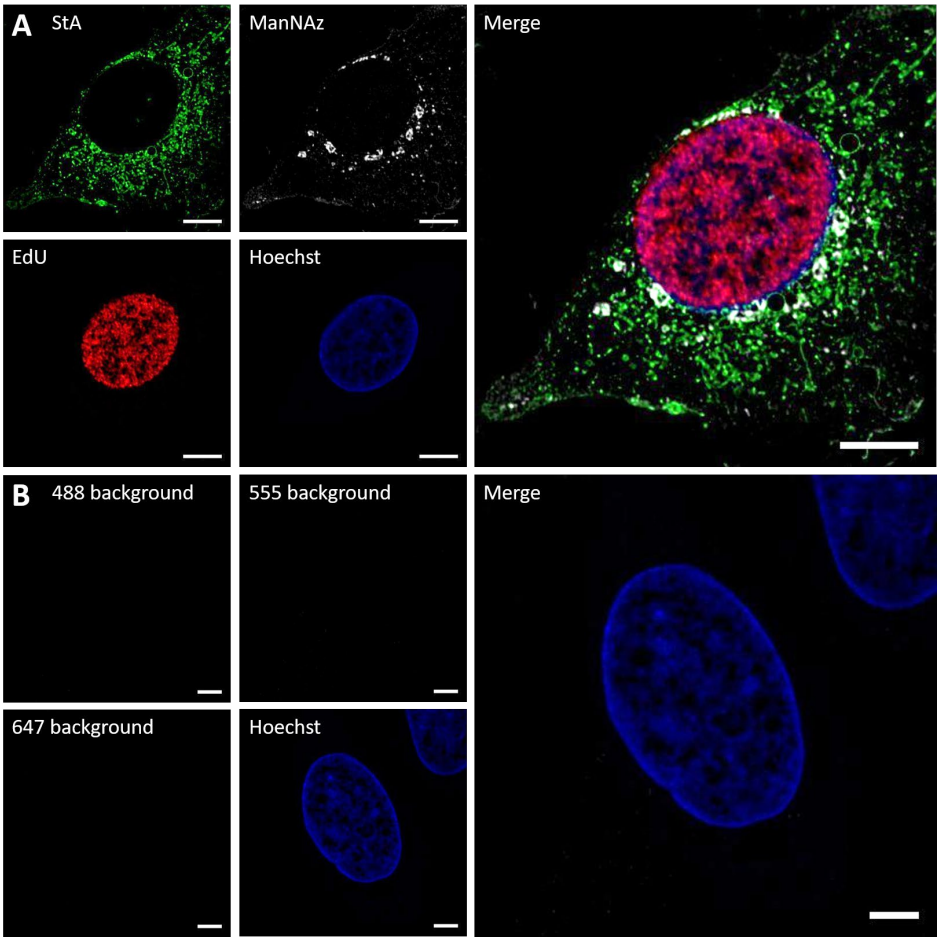

Figure 15. Triple orthogonal bioorthogonal labeling (triple click), studied by confocal microscopy. (**A**) U2OS cells were incubated with StA (green), Ac4ManNAz (gray) and EdU (red) simultaneously for two hours, and visualized through sequential triple click reactions using AFDye 488-tetrazine, AFDye 555-alkyne and AFDye 647-azide, with intermediate washing. (**B**) U2OS cells were incubated without labels for two hours, and background labeling was analyzed by subjecting the unlabeled cells to the same triple click treatment as above. DNA was counterstained with Hoechst for reference. Scale bar represents 5 µm.

6.3 Challenges and limitations of the current B-CLEM approach

Although bioorthogonal labeling has proven to be a useful partner for various fluorescence-based analysis and imaging techniques, including CLEM, it does introduce some intrinsic challenges and limitations. First of all, the introduction of a click handle through metabolic labeling can be challenging, depending on the biomolecule and organism of interest. For example, it has been shown that while bioorthogonal analogues of mannosamine and various other sugars are readily metabolized and incorporated into cell surface glycans, analogues of galactose are not.[51] This hurdle could be overcome by injecting a bioorthogonal analogue of a downstream metabolite (UDP-galactose) but clearly exemplifies how a single approach cannot always be translated directly to similar biomolecules. Similarly, while bioorthogonal analogues of D-alanine are readily incorporated into the peptidoglycan of many bacteria, *Chlamydia trachomatis* does not accept D-alanine analogues.[52] Again, this hurdle could be overcome by using a bioorthogonal analogues of a downstream metabolite (D-alanine-D-alanine dipeptide) but it exemplifies how a potential difference between organisms.

Another challenge is the selective ligation of a fluorophore to the incorporated click handle, which starts with selecting a suitable bioorthogonal reaction. The ccHc reaction is a logical first choice, since the alkyne and azide groups are the smallest available click handles, resulting in minimal interference in the function of the labeled biomolecule. The reaction is also fast, selective (low background) and well-established. However, the copper(I)-dependency of this reaction makes it unsuitable for live cell ligation and causes several problems for copper/redox-sensitive techniques. The copper-free spHc reaction can be used to avoid this issue but at the expense of speed and selectivity. An IEDDA reaction provides a viable alternative but at the expense of click handle size, potentially causing interference in the function of the biomolecule of interest.

Performing the ligation reaction can bring challenges as well. Whereas cell surface labels can easily be reached by a fluorophore in solution, an intracellular click handle requires additional consideration. Cell permeable fluorophores are often poorly water soluble, causing additional background labeling, while water soluble fluorophores are often cell impermeable. It is therefore desirable to chemically fix and permeabilize (or section) the cells in order to allow fluorophores to freely access the intracellular environment. If live cell imaging

is required, a compatible reaction should be chosen, in combination with a cell permeable fluorophore.

Since electron microscopy requires fixation of the biological sample, all available bioorthogonal reactions should theoretically be compatible with CLEM. However, only the Tokuyasu cryo-sectioning method has thus far been proven to be compatible with on-section click reactions.[17] Other techniques usually involve resin embedding, for which the click handles are expected to either be degraded in the polymerization process or become unreachable for the fluorophore.[53] It is important to note that cryo-sectioning provides poorer contrast and preservation of ultrastructure when comparing to resin-based methods.[54] It would therefore be beneficial to identify a method that is compatible with bioorthogonal ligation reactions, while providing better contrast and preservation of ultrastructure. A recent publication showed that, surprisingly, immunogold labeling can still be performed on ultrathin sections of resin-embedded cells.[54] Therefore, if a mild resin-embedding method can be identified that is compatible with click handles, this could potentially open up new possibilities for on-section click reactions as well. Alternatively, if the bioorthogonal ligation reactions are performed on live cells, the cells could then be fixed and resin-embedded, potentially providing better contrast and preservation of ultrastructure (assuming the fluorescence is preserved).[55]

STORM-CLEM provides roughly 10-fold better spatial resolution in the fluorescent signal and much higher sensitivity compared to confocal-CLEM.[56] However, this technique introduces several additional challenges and limitations. Whereas the entire process of sample preparation, cryo-sectioning, imaging and correlation of images for CLEM is already highly laborious, the addition of STORM makes the process even more laborious and time consuming. Additionally, due to the single-molecule sensitivity of STORM, the observable background labeling of non-specifically bound fluorophores is increased significantly.[57] Reduction of this background is highly desirable but difficult to achieve. Finally, the high laser power required for STORM has a negative effect on the preservation of ultrastructure.[57] It would therefore be desirable to use an alternative super-resolution fluorescence microscopy technique that requires lower laser power, such as DNA-based point accumulation for imaging in nanoscale topography (DNA-PAINT) in combination with on-section click reactions.[58]

6.4 Conclusion and future outlook

In summary, the current B-CLEM method can be applied to many different research questions and still has a lot of room for improvements. Its broad compatibility with many labeling strategies, as well as the potential for direct translation to bioorthogonal STORM-CLEM, flow cytometry and other techniques, is a great virtue. Nevertheless, alternative strategies combining click chemistry with CLEM can be conceived, in order to overcome intrinsic limitations of the current technique.

First, 3D information could also be obtained with CLEM. To achieve this, a large series of sections must be obtained, individually correlated, and manually stacked in a retrospective manner, known as array tomography. Although not impossible, this is very difficult to achieve with Tokuyasu cryo-sections. A different approach would be to perform the click reaction(s) on live cells, followed by resin embedding and room-temperature sectioning to obtain strong, consistent sections that are more suited for array tomography.[55]

Second, the need for chemical fixation can be overcome by using cryo-EM. To achieve this, the click reaction(s) must be performed on live cells, after which the sample is plunge-frozen. Super-resolution cryo-CLEM can then be performed to obtain high-resolution fluorescence information within the native ultrastructure.[59,60]

Finally, the need for electron microscopy may be circumvented by using of expansion microscopy.[61] Although technically not CLEM, this technique uses physical swelling of the sample to enlarge the cells enough to obtain EM-resolution using only light microscopy.[62]

It is important to note that all three examples have limitations of their own, such as the need to perform the click reactions on live cells, rendering the ccHc reaction nearly impossible. Therefore, when the small size of the incorporated click handles is a priority, the current B-CLEM method is still preferred.

6.5 Experimental

Safety statement

All biological experiments with *S. enterica* serovar Typhimurium described in this study were performed under strict Bio Safety Level 2 conditions. Following fixation and disinfection of the tubes, further sample preparation for CLEM was performed under normal laboratory conditions. No unexpected or unusually high safety hazards were encountered.

Reagents

Lysogeny broth (LB) medium, methionine (Met), Dulbecco's modified Eagle medium (DMEM), Iscove's Modified Dulbecco's Medium (IMDM), GlutaMAX, pyruvate, 4-(2-hydroxyethyl)-1-piperazineethanesulfonic acid (HEPES), glycine, gelatin type A bloom 300 (gelatin), paraformaldehyde (PFA), bovine serum albumin (BSA), Copper(II) sulfate pentahydrate, (+)-sodium L-ascorbate, tris(3-hydroxypropyltriazolylmethyl)amine (THPTA), aminoguanidine hydrochloride, and IGEPAL CA-630 were purchased from Sigma-Aldrich, Zwijndrecht, The Netherlands. Non-essential amino acids (NEAA), 2-mercaptoethanol, L-glutamine, Hoechst 33342, 4',6-Diamidino-2-Phenylindole (DAPI) and Alexa Fluor 488 (AF488)-alkyne were purchased from Thermo Fisher Scientific, Bleiswijk, The Netherlands. AFDye488-tetrazine, AFDye555-alkyne and AFDye647-azide were purchased from Click Chemistry Tools, Scottsdale, USA. SelenoMet minimal medium was purchased from Molecular Dimensions, Sheffield, UK. D-propargylglycine (alkDala) was purchased from Combi-Blocks, San Diego, USA. EM-grade 8% paraformaldehyde, EM-grade 8% glutaraldehyde and BSA-c were purchased from Aurion, Wageningen, The Netherlands. Fetal calf serum (FCS) was purchased from VWR International, Amsterdam, The Netherlands. Penicillin G sodium and streptomycin sulphate were purchased from Duchefa, Haarlem, The Netherlands. Granulocyte-Macrophage Colony-Stimulating Factor (GM-CSF) was purchased from ImmunoTools, Friesoythe, Germany. BMV109 and FJD239 were kindly provided by Floris van Dalen and Dr. Martijn Verdoes.

Organic synthesis

Synthesis of (S)-2-Aminohex-5-ynoic acid (L-homopropargylglycine; Hpg)

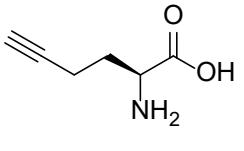

Hpg was synthesized according to previously described procedure by Li et al.[63], adjusted to obtain the enantiomerically pure L-Hpg variant based on Chenault et al.[64], Biagini et al.[65] and Dong et al.[66]

Chiral deprotection of *N*-acetyl-DL-homopropargylglycine (2-acetamidohex-5-ynoic acid)

A solution of 303 mg (1.13 mmol, 1 eq.) *N*-acetyl-DL-homopropargylglycine in 20 mL H_2O and adjusted to pH 7.5 using 1M NH_4OH. 1 mg kidney acylase I (≥2000 units/mg) was added and the mixture was stirred for 16 h at 37°C. The enzyme was recovered by centrifugation dialysis, using a 10kDa membrane at 4000 rpm for 35 min at 10°C. Next, the solution was acidified to pH 3 with 2M HCl and extracted with 3 x 20 mL diethyl ether. The organic layers were concentrated to retrieve the *N*-acetyl-D-homopropargylglycine. The aqueous layer was loaded on a pre-washed and regenerated Dowex 50WX8 cation exchange resin (60 mL). The column was washed with 5 x bed volume of water, maintaining a pH of 5.5 at the exit and eluted with 200 mL 1.5M NH_4OH. Product was detected by TLC and the eluate was concentrated and lyophilized to yield chirally pure L-Hpg (68 mg, 0.535 mmol, 95%) as a white powder.

^{1}H NMR (400MHz, D_2O): δ [ppm] = 4.11 (t, J = 6.4 Hz, 1H), 2.42 – 2.36 (m, 2H), 2.36 (s, 1H), 2.19 – 2.10 (m, 1H), 2.07 – 1.98 (m, 1H); 13C NMR (101MHz, D2O): δ 82.28, 71.16, 52.05, 28.44, 14.16; HRMS (ESI): $C_6H_9NO_2$ $[M+H]^+$ 128.06, found 128.07; $[\alpha]_{20}^{D}$: +32.4 (c = 1, 1 M HCl); Ref [66]: +28 (c = 1, 1 M HCl).

Bacterial culture and metabolic labeling

E. coli B834, *E. coli* B834 expressing GFP[17] and *Stm* SL1344 expressing DsRed[67] were grown overnight at 37°C in LB medium. The following day cultures were diluted 1:33 and grown at 37°C to an OD_{600} between 0.3-0.5. In case of metabolic labeling, the bacteria were collected and resuspended in SelenoMet medium, supplemented with 4 mM Hpg and incubated for 30 min at 37°C to allow for label incorporation. The bacteria were washed (1x PBS), resuspended in PBS and their concentration was measured by OD_{600}. Throughout culturing, the medium was supplemented with 100 µg/ml ampicillin.

Mammalian cell culture

U2OS cells were cultured in DMEM, supplemented with with 10% heat-inactivated FCS, 2 mM GlutaMAX, penicillin 100 I.U./mL and streptomycin 50 µg/mL.

DC2.4 and D1 cells were cultured in IMDM, supplemented with 10% heat-inactivated FCS, 2 mM GlutaMAX, 10 mM HEPES pH 7.3, 1 mM pyruvate, penicillin 100 I.U./mL and streptomycin 50 µg/mL, 50 µM 2-Mercaptoethanol and 1X non-essential amino acids. D1 cells were additionally supplemented with fibroblast supernatant from NIH/3T3 cells, collected from confluent cultures and filtered.

Mouse bone marrow-derived dendritic cells (BMDCs) were generated from B57BL/6 mice bone marrow essentially as described[68] with some modifications. Briefly, bone marrow was flushed from femurs and tibia and cells were cultured in IMDM supplemented with 8% heat-inactivated FCS, 2 mM L-glutamine, 20 µM 2-Mercaptoethanol, penicillin 100 I.U./mL and streptomycin 50 µg/mL in the presence of 20 ng/mL GM-CSF. Medium was replaced on day 3 and 7 of culture and the cells were used between days 10 and 13.

Infection with Hpg-labeled *E. coli* and incubation with Activity-Based Probes

For confocal microscopy, 2 x 10^5 BMDCs were seeded on an 8-chamber slide (Ibidi) and left to attach for 3 hours. For CLEM, 10 x 10^6 BMDCs were seeded on a 10 cm dish and left to attach for 3 hours. Infection of dendritic cells was achieved by adding Hpg-labeled *E. coli* at an MOI of 50 and incubating for 45 min at 37°C, 5% CO_2. Unbound/non-internalized bacteria were washed off (2x PBS) and medium was replaced for immediate analysis (t = 0) or further incubation for 1 or 3 hours. The cells were then incubated for 1 hour with 100 nM FJD239 and washed (2x PBS). Next, the cells were additionally incubated for 1 hour with 1 µM BMV109 and washed (2x PBS).

Infection with *E. coli* and/or *Stm* and incubation with Activity-Based Probes

For confocal microscopy, 5 x 10^4 DC2.4 cells were seeded on an 8-chamber slide (Ibidi) and left to grow overnight. For CLEM, 10 x 10^6 D1 cells were seeded on a 10 cm dish and left to attach for 3 hours. Infection of dendritic cells was achieved by adding GFP-expressing *E. coli* and/or DsRed-expressing *Stm* at an MOI of 50 and incubating for 45 min at 37°C, 5% CO_2. Unbound/non-internalized bacteria were washed off (2x PBS) and medium was replaced for immediate analysis (t = 0) or further incubation for 1 or 3 hours. The cells were then additionally incubated for 1 hour with 1 µM BMV109 and washed (2x PBS).

Triple bioorthogonal metabolic labeling

For confocal microscopy, 2 x 10^5 U2OS cells were seeded on an 8-chamber slide (Ibidi) and left to attach for 3 hours. A metabolic label cocktail was prepared, containing 100 µM sterculic acid (StA), 100 µM 1,3,4,6-tetra-*O*-acetyl-*N*-

azidoacetylmannosamine (Ac4ManNAz) and 10 µM 5-Ethynyl-2'-deoxyuridine (EdU) in cell medium. The cells were incubated with metabolic label cocktail for 2 hours at 37°C, 5% CO_2, additionally incubated with fresh cell medium for 15 min to allow for diffusion of non-incorporated metabolic labels and washed (2x PBS).

Preparation for whole cell confocal microscopy

Following the biological experiment, the cells were fixed for 2 hours in 4% PFA at RT, then kept in 0.5% PFA at 4°C until further processing. Fixed cells were then washed with PBS and 20 mM glycine in PBS to quench potential aldehyde residues. Cells containing click handles were then permeabilized for 20 min with 0.1% Triton-X100 and washed (1x PBS).

Samples without click handles were immediately counterstained with 2 µg/mL Hoechst 33342 in PBS for 5 min and washed once more with PBS, without additional staining.

Samples containing an azide (FJD239) and an alkyne (Hpg-*E. coli*) functionality were first reacted with 5 µM AFDye555-azide in ccHc cocktail (0.1 M HEPES, pH 7.3, 1 mM $CuSO_4$, 10 mM sodium ascorbate, 1 mM THPTA ligand, 10 mM amino-guanidine) for 1 hour, washed (2x PBS) and subsequently reacted with 5 µM AF488-alkyne in ccHc cocktail.

Samples containing a cyclopropene (StA), an azide (Ac4ManNAz) and an alkyne (EdU) functionality were first reacted with 5 µM AFDye488-tetrazine in PBS, washed (2x PBS), then reacted with 5 µM AFDye647-azide in ccHc cocktail, washed (2x PBS) and finally reacted with 5 µM AFDye555-alkyne in ccHc cocktail.

After the click reactions, the cells were washed (1x PBS) and incubated for 30 min with 1% BSA in PBS to facilitate removal of non-specifically bound fluorophores, and washed (1x PBS). Nuclei were counterstained with 2 µg/mL Hoechst 33342 for 5 min and washed once more with PBS. All samples were imaged in glycerol/DABCO solution to minimize photobleaching.

Preparation of dendritic cells for CLEM

Following the biological experiment, the cells were fixed for 24 hours in 2% EM-grade PFA in 0.1M phosphate buffer pH 7.2 at RT, then kept in 0.5% EM-grade PFA at 4°C until further processing. Fixed cells were rinsed with PBS, harvested in warm 1% gelatin in PBS with cell scrapers and transferred to a 15 mL Falcon tube. The cells were collected by centrifugation, resuspended in warm 1% gelatin in PBS, transferred to a 1.5 mL Eppendorf tube, resuspended in warm 12% gelatin in PBS

and pelleted by centrifugation (3 min at 800 rcf). After jellification on ice, the sample pellet was cut off from the tube and cut in half with a razor knife. Sample cubes of approx. 1 mm^2 were prepared and rotated in a 2.3 M sucrose solution for 18 hours to allow for sucrose infiltration, as a cryo-protectant, followed by plunge-freezing the cubes on metal support pins.

Cryo-sectioning and on-section ccHc reaction

Ultrathin (75 nm) cryo-sections were prepared according to the Tokuyasu technique [69,70], using a cryo-ultramicrotome (Leica) and diamond knife (Diatome). Sections were thawed on a droplet of pickup fluid (1.15 M sucrose, 1% methylcellulose) and transferred to a Formvar/carbon-coated TEM grid (titanium, 100 square mesh, 3.05 mm, center-marked; Agar Scientific), pre-coated with blue 0.2 µm FluoSpheres (Thermo Fisher) as fiducial markers. Thawed cryo-sections attached to the TEM grid were incubated on 2% gelatin in PBS for 30 min at 37°C, followed by washing on 20 mM glycine in PBS (5x 2 min).

Samples without click handles were immediately counterstained with 0.2 µg/mL DAPI in PBS for 5 min and washed once more with PBS without additional staining.

Samples containing an azide (FJD239) and an alkyne (Hpg-*E. coli*) functionality were first reacted with 5 µM AFDye555-azide in ccHc cocktail (0.1 M HEPES, pH 7.3, 1 mM $CuSO_4$, 10 mM sodium ascorbate, 1 mM THPTA ligand, 10 mM amino-guanidine) for 1 hour, washed (2x PBS) and subsequently reacted with 5 µM AF488-alkyne in ccHc cocktail. These samples were then incubated on 1% BSA in PBS (3x 10 min), to assist the removal of non-specifically bound fluorophores and additionally blocked on 0.1% BSA-c in PBS (2x 2 min). Immunogold staining was achieved by 1 hour incubation on anti-LAMP1 (1D4B, 1:300, eBioscience) or anti-MHC II (M5/114, 1:300, BioXCell), followed by washing (2x 0.1% BSA-c in PBS), 20 min incubation on rabbit-anti-rat (1:50, Abcam), washing (2x 0.1% BSA-c in PBS), 20 min incubation on protein-A conjugated to 15 nm gold (1:50; Aurion). These samples were then washed (2x 0.1% BSA-c in PBS and 3x PBS), followed by immobilization of the antibody complexes by incubating 5 min on 1% glutaraldehyde in PBS. The samples were then washed (3x PBS), counterstained with 0.2 µg/mL DAPI in PBS for 5 min and washed once more (3x milliQ H_2O).

The fluorescently-labeled sections attached to TEM grids were mounted in water containing 30% glycerol between a microscopy slide and a coverslip, and sealed with silver Scotch tape.

Confocal microscopy

All samples were imaged on an Andor Dragonfly 505 Spinning Disk Confocal (Oxford Instruments), containing an 8-line integrated laser engine, on a Leica DMi8 inverted microscope equipped with a 63X/1.40-0.60 HCX PL APO oil objective or 100X/1.47 HC PL APO TIRF-corrected oil objective. Hoechst, DAPI and FluoSpheres were excited with the 405 line and collected with the 450/50 BP emission filter, AF488 was excited with the 488 line and collected with the 525/50 BP emission filter, DsRed was excited with the 561 line and collected with the 620/60 BP emission filter and AF647 was excited with the 637 line and collected with the 700/75 BP emission filter. Images were acquired with the Zyla 2048x2048 sCMOS camera and 2x2 camera binning controlled with the integrated Fusion software. Z-series optical sections were collected with a system-optimized step-size of 0.13 microns and deconvolved using the integrated ClearView-GPU™ deconvolution software. Gamma, brightness and contrast were carefully adjusted (identically for compared image sets) using FIJI.[71] In case of CLEM, maximum intensity projections were made, in order to compensate for non-flat sections.

TEM imaging and correlation

After acquiring the confocal fluorescence microscopy (FM) images, the TEM grids containing the sections were recovered from the microscopy slides, rinsed in milliQ water and incubated for 5 min on droplets of uranyl acetate/methylcellulose. The negatively-stained sections were then imaged on a FEI Tecnai 12 BioTwin TEM System (FEI Technologies) at 120 kV acceleration voltage. Correlation of FM to TEM images was performed in Adobe Photoshop CC 2020 (Adobe Systems). The separate fluorescence channels were imported as layers, set to overlay mode 'Lighten', then grouped and set to overlay mode 'Color', placed on top of the TEM image. Transformation of the FM image to match the TEM image was achieved by isotropic scaling with interpolation setting 'bicubic smoother', translation and rotation. Alignment at low magnification was guided by the grid bars and nuclei. Alignment at high magnification was guided by the shape of the nucleus and the position of the fiducial beads.

6.6 References

(1) Jakoš, T.; Pišlar, A.; Jewett, A.; Kos, J. Cysteine Cathepsins in Tumor-Associated Immune Cells. *Frontiers in Immunology*. Frontiers Media S.A. August 28, 2019, p 2037.

(2) Gupta, S.; Singh, R. K.; Dastidar, S.; Ray, A. *Cysteine Cathepsin S as an Immunomodulatory Target: Present and Future Trends*; Taylor & Francis, 2008; Vol. 12, pp 291–299.

(3) Fonović, M.; Turk, B. Cysteine Cathepsins and Extracellular Matrix Degradation. *Biochimica et Biophysica Acta - General Subjects*. Elsevier August 1, 2014, pp 2560–2570.

(4) Sevenich, L.; Bowman, R. L.; Mason, S. D.; Quail, D. F.; Rapaport, F.; Elie, B. T.; Brogi, E.; Brastianos, P. K.; Hahn, W. C.; Holsinger, L. J.; Massagué, J.; Leslie, C. S.; Joyce, J. A. Analysis of Tumour- and Stroma-Supplied Proteolytic Networks Reveals a Brain-Metastasis-Promoting Role for Cathepsin S. *Nat. Cell Biol.* **2014**, *16* (9), 876–888.

(5) Sobotič, B.; Vizovišek, M.; Vidmar, R.; Van Damme, P.; Gocheva, V.; Joyce, J. A.; Gevaert, K.; Turk, V.; Turk, B.; Fonović, M. Proteomic Identification of Cysteine Cathepsin Substrates Shed from the Surface of Cancer Cells. *Mol. Cell. Proteomics* **2015**, *14* (8), 2213–2228.

(6) Driessen, C.; Bryant, R. A. R.; Lennon-Duménil, A. M.; Villadangos, J. A.; Bryant, P. W.; Shi, G. P.; Chapman, H. A.; Ploegh, H. L. Cathepsin S Controls the Trafficking and Maturation of MHC Class II Molecules in Dendritic Cells. *J. Cell Biol.* **1999**, *147* (4), 775–790.

(7) Shen, L.; Sigal, L. J.; Boes, M.; Rock, K. L. Important Role of Cathepsin S in Generating Peptides for TAP-Independent MHC Class I Crosspresentation in Vivo. *Immunity* **2004**, *21* (2), 155–165.

(8) Bania, J.; Gatti, E.; Lelouard, H.; David, A.; Cappello, F.; Weber, E.; Camosseto, V.; Pierre, P. Human Cathepsin S, but Not Cathepsin L, Degrades Efficiently MHC Class II-Associated Invariant Chain in Nonprofessional APCs. *Proc. Natl. Acad. Sci. U. S. A.* **2003**, *100* (11), 6664–6669.

(9) Theron, M.; Bentley, D.; Nagel, S.; Manchester, M.; Gerg, M.; Schindler, T.; Silva, A.; Ecabert, B.; Teixeira, P.; Perret, C.; Reis, B. Pharmacodynamic Monitoring of RO5459072, a Small Molecule Inhibitor of Cathepsin S. *Front. Immunol.* **2017**, *8* (JUL), 806.

(10) Oresic Bender, K.; Ofori, L.; Van Der Linden, W. A.; Mock, E. D.; Datta, G. K.; Chowdhury, S.; Li, H.; Segal, E.; Sanchez Lopez, M.; Ellman, J. A.; Figdor, C. G.; Bogyo, M.; Verdoes, M. Design of a Highly Selective Quenched Activity-Based Probe and Its Application in Dual Color Imaging Studies of Cathepsin S Activity Localization. *J. Am. Chem. Soc.* **2015**, *137* (14), 4771–4777.

(11) van Dalen, F. J.; Bakkum, T.; van Leeuwen, T.; Groenewold, M.; Deu, E.; Koster, A.; Van Kasteren, S. I.; Verdoes, M. Application of a Highly Selective Cathepsin S Two-Step Activity-Based Probe in Multicolour Bio-Orthogonal Correlative Light Electron Microscopy. *Front. Chem.* **2020**, *8* (628433), 1–13.

(12) Helft, J.; Böttcher, J.; Chakravarty, P.; Zelenay, S.; Huotari, J.; Schraml, B. U.; Goubau, D.; Reis e Sousa, C. GM-CSF Mouse Bone Marrow Cultures Comprise a Heterogeneous Population of CD11c+MHCII+ Macrophages and Dendritic Cells. *Immunity* **2015**, *42* (6), 1197–1211.

(13) Mayhew, T. M.; Lucocq, J. M. Multiple-Labelling ImmunoEM Using Different Sizes of Colloidal Gold: Alternative Approaches to Test for Differential Distribution and Colocalization in Subcellular Structures. *Histochem. Cell Biol.* **2011**, *135* (3), 317–326.

(14) Eissing, N.; Heger, L.; Baranska, A.; Cesnjevar, R.; Büttner-Herold, M.; Söder, S.; Hartmann, A.; Heidkamp, G. F.; Dudziak, D. Easy Performance of 6-Color Confocal

Immunofluorescence with 4-Laser Line Microscopes. *Immunol. Lett.* **2014**, *161* (1), 1–5.
(15) Luzio, J. P.; Pryor, P. R.; Bright, N. A. Lysosomes: Fusion and Function. *Nat. Rev. Mol. Cell Biol.* **2007**, *8* (8), 622–632.
(16) Flannagan, R. S.; Jaumouillé, V.; Grinstein, S. The Cell Biology of Phagocytosis. *Annu. Rev. Pathol. Mech. Dis.* **2012**, *7* (1), 61–98.
(17) van Elsland, D. M.; Bos, E.; de Boer, W.; Overkleeft, H. S.; Koster, A. J.; van Kasteren, S. I. Detection of Bioorthogonal Groups by Correlative Light and Electron Microscopy Allows Imaging of Degraded Bacteria in Phagocytes. *Chem. Sci.* **2016**, *7* (1), 752–758.
(18) Uribe-Quero, E.; Rosales, C. Control of Phagocytosis by Microbial Pathogens. *Front. Immunol.* **2017**, *8* (OCT), 1–23.
(19) Blum, J. S.; Wearsch, P. A.; Cresswell, P. Pathways of Antigen Processing. *Annu. Rev. Immunol.* **2013**, *31* (1), 443–473.
(20) Kleijmeer, M.; Ramm, G.; Schuurhuis, D.; Griffith, J.; Rescigno, M.; Ricciardi-Castagnoli, P.; Rudensky, A. Y.; Ossendorp, F.; Melief, C. J. M.; Stoorvogel, W.; Geuze, H. J. Reorganization of Multivesicular Bodies Regulates MHC Class II Antigen Presentation by Dendritic Cells. *J. Cell Biol.* **2001**, *155* (1), 53–63.
(21) Bosch, B.; Berger, A. C.; Khandelwal, S.; Heipertz, E. L.; Scharf, B.; Santambrogio, L.; Roche, P. A. Disruption of Multivesicular Body Vesicles Does Not Affect Major Histocompatibility Complex (MHC) Class II-Peptide Complex Formation and Antigen Presentation by Dendritic Cells. *J. Biol. Chem.* **2013**, *288* (34), 24286–24292.
(22) van Leeuwen, T.; Araman, C.; Pieper Pournara, L.; Kampstra, A. S. B.; Bakkum, T.; Marqvorsen, M. H. S.; Nascimento, C. R.; Groenewold, G. J. M.; van der Wulp, W.; Camps, M. G. M.; Janssen, G. M. C.; van Veelen, P. A.; van Westen, G. J. P.; Janssen, A. P. A.; Florea, B. I.; Overkleeft, H. S.; Ossendorp, F. A.; Toes, R. E. M.; van Kasteren, S. I. Bioorthogonal Protein Labelling Enables the Study of Antigen Processing of Citrullinated and Carbamylated Auto-Antigens. *RSC Chem. Biol.* **2021**.
(23) Pawlak, J. B.; Gential, G. P. P.; Ruckwardt, T. J.; Bremmers, J. S.; Meeuwenoord, N. J.; Ossendorp, F. A.; Overkleeft, H. S.; Filippov, D. V.; Van Kasteren, S. I. Bioorthogonal Deprotection on the Dendritic Cell Surface for Chemical Control of Antigen Cross-Presentation. *Angew. Chemie - Int. Ed.* **2015**, *54* (19), 5628–5631.
(24) van der Gracht, A. M. F.; de Geus, M. A. R.; Camps, M. G. M.; Ruckwardt, T. J.; Sarris, A. J. C.; Bremmers, J.; Maurits, E.; Pawlak, J. B.; Posthoorn, M. M.; Bonger, K. M.; Filippov, D. V; Overkleeft, H. S.; Robillard, M. S.; Ossendorp, F.; van Kasteren, S. I. Chemical Control over T-Cell Activation In Vivo Using Deprotection of Trans-Cyclooctene-Modified Epitopes. *ACS Chem. Biol.* **2018**, acschembio.8b00155.
(25) Bagert, J. D.; Xie, Y. J.; Sweredoski, M. J.; Qi, Y.; Hess, S.; Schuman, E. M.; Tirrell, D. A. Quantitative, Time-Resolved Proteomic Analysis by Combining Bioorthogonal Noncanonical Amino Acid Tagging and Pulsed Stable Isotope Labeling by Amino Acids in Cell Culture. *Mol. Cell. Proteomics* **2014**, *13* (5), 1352–1358.
(26) Thakur, A.; Mikkelsen, H.; Jungersen, G. Intracellular Pathogens: Host Immunity and Microbial Persistence Strategies. *Journal of Immunology Research*. Hindawi Limited 2019.
(27) Buchmeier, N. A.; Heffron, F. Inhibition of Macrophage Phagosome-Lysosome Fusion by Salmonella Typhimurium. *Infect. Immun.* **1991**, *59* (7), 2232–2238.
(28) Pradhan, D.; Pradhan, J.; Mishra, A.; Karmakar, K.; Dhiman, R.; Chakravortty, D.; Negi, V. D. Immune Modulations and Survival Strategies of Evolved Hypervirulent Salmonella Typhimurium Strains. *Biochim. Biophys. Acta - Gen. Subj.* **2020**, 129627.
(29) Gray, M. A.; Choy, C. H.; Dayam, R. M.; Ospina-Escobar, E.; Somerville, A.; Xiao, X.; Ferguson, S. M.; Botelho, R. J. Phagocytosis Enhances Lysosomal and Bactericidal Properties by Activating the Transcription Factor TFEB. *Curr. Biol.* **2016**, *26* (15), 1955–1964.

(30) Bah, A.; Vergne, I. Macrophage Autophagy and Bacterial Infections. *Frontiers in Immunology*. Frontiers Media S.A. November 6, 2017, p 1483.
(31) Azimi, T.; Zamirnasta, M.; Sani, M. A.; Dallal, M. M. S.; Nasser, A. Molecular Mechanisms of Salmonella Effector Proteins: A Comprehensive Review. *Infection and Drug Resistance*. Dove Medical Press Ltd. January 6, 2020, pp 11–26.
(32) Kaper, J. B.; Nataro, J. P.; Mobley, H. L. T. Pathogenic Escherichia Coli. *Nature Reviews Microbiology*. Nature Publishing Group February 2004, pp 123–140.
(33) Sletten, E. M.; Bertozzi, C. R. From Mechanism to Mouse; A Tale of Two Bioorthogonal Reactions. *Acc. Chem. Res.* **2011**, *44* (9), 666–676.
(34) Saxon, E.; Bertozzi, C. R. Cell Surface Engineering by a Modified Staudinger Reaction. *Science* **2000**, *287* (5460), 2007–2010.
(35) Patterson, D. M.; Prescher, J. A. Orthogonal Bioorthogonal Chemistries. *Curr. Opin. Chem. Biol.* **2015**, *28*, 141–149.
(36) Nguyen, S. S.; Prescher, J. A. Developing Bioorthogonal Probes to Span a Spectrum of Reactivities. *Nat. Rev. Chem.* **2020**, *4* (9), 476–489.
(37) Willems, L. I.; Li, N.; Florea, B. I.; Ruben, M.; Van Der Marel, G. A.; Overkleeft, H. S. Triple Bioorthogonal Ligation Strategy for Simultaneous Labeling of Multiple Enzymatic Activities. *Angew. Chemie - Int. Ed.* **2012**, *51* (18), 4431–4434.
(38) Narayanam, M. K.; Liang, Y.; Houk, K. N.; Murphy, J. M. Discovery of New Mutually Orthogonal Bioorthogonal Cycloaddition Pairs through Computational Screening. *Chem. Sci.* **2016**, *7* (2), 1257–1261.
(39) Liang, Y.; Mackey, J. L.; Lopez, S. A.; Liu, F.; Houk, K. N. Control and Design of Mutual Orthogonality in Bioorthogonal Cycloadditions. *J. Am. Chem. Soc.* **2012**, *134* (43), 17904–17907.
(40) Karver, M. R.; Weissleder, R.; Hilderbrand, S. A. Bioorthogonal Reaction Pairs Enable Simultaneous, Selective, Multi-Target Imaging. *Angew. Chemie - Int. Ed.* **2012**, *51* (4), 920–922.
(41) Rahim, M. K.; Kota, R.; Haun, J. B. Enhancing Reactivity for Bioorthogonal Pretargeting by Unmasking Antibody-Conjugated Trans -Cyclooctenes. *Bioconjug. Chem.* **2015**, *26* (2), 352–360.
(42) Worrell, B. T.; Malik, J. A.; Fokin, V. V. Direct Evidence of a Dinuclear Copper Intermediate in Cu(I)-Catalyzed Azide-Alkyne Cycloadditions. *Science (80-.).* **2013**, *340*, 457–460.
(43) Matikonda, S. S.; Orsi, D. L.; Staudacher, V.; Jenkins, I. A.; Fiedler, F.; Chen, J.; Gamble, A. B. Bioorthogonal Prodrug Activation Driven by a Strain-Promoted 1,3-Dipolar Cycloaddition. *Chem. Sci.* **2015**, *6* (2), 1212–1218.
(44) Oliveira, B. L.; Guo, Z.; Bernardes, G. J. L. Inverse Electron Demand Diels–Alder Reactions in Chemical Biology. *Chem. Soc. Rev.* **2017**, *46* (16), 4895–4950.
(45) Ramil, C. P.; Lin, Q. Bioorthogonal Chemistry: Strategies and Recent Developments. *Chem. Commun.* **2013**, *49* (94), 11007–11022.
(46) Sarris, A. J.; Hansen, T.; de Geus, M. A.; Maurits, E.; Doelman, W.; Overkleeft, H. S.; Codee, J. D.; Filippov, D.; van Kasteren, S. I. Fast and PH Independent Elimination of Trans-Cyclooctene Using Aminoethyl Functionalized Tetrazines. *Chem. - A Eur. J.* **2018**.
(47) Rieder, U.; Luedtke, N. W. Alkene-Tetrazine Ligation for Imaging Cellular DNA. *Angew. Chemie - Int. Ed.* **2014**, *53* (35), 9168–9172.
(48) Lang, K.; Chin, J. W. Bioorthogonal Reactions for Labeling Proteins. *ACS Chem. Biol.* **2014**, *9* (1), 16–20.
(49) Devaraj, N. K. The Future of Bioorthogonal Chemistry. *ACS Cent. Sci.* **2018**, *4*, 952–959.
(50) Shang, X.; Lai, R.; Song, X.; Li, H.; Niu, W.; Guo, J. Improved Photoinduced Fluorogenic Alkene-Tetrazole Reaction for Protein Labeling. *Bioconjug. Chem.* **2017**, *28* (11), 2859–2864.

(51) Daughtry, J. L.; Cao, W.; Ye, J.; Baskin, J. M. Clickable Galactose Analogues for Imaging Glycans in Developing Zebrafish. *ACS Chem. Biol.* **2020**.

(52) Liechti, G. W.; Kuru, E.; Hall, E.; Kalinda, A.; Brun, Y. V.; Vannieuwenhze, M.; Maurelli, & A. T.; Maurelli, A. T. A New Metabolic Cell-Wall Labelling Method Reveals Peptidoglycan in Chlamydia Trachomatis. *Nature* **2014**, *506* (7489), 507–510.

(53) van Elsland, D. M.; van Kasteren, S. I. Imaging Bioorthogonal Groups in Their Ultrastructural Context with Electron Microscopy. *Angew. Chemie - Int. Ed.* **2016**, *55* (33), 9472–9473.

(54) Flechsler, J.; Heimerl, T.; Pickl, C.; Rachel, R.; Stierhof, Y. D.; Klingl, A. 2D and 3D Immunogold Localization on (Epoxy) Ultrathin Sections with and without Osmium Tetroxide. *Microsc. Res. Tech.* **2020**, *83* (6), 691–705.

(55) Peters, S.; Kaiser, L.; Fink, J.; Schumacher, F.; Perschin, V.; Schlegel, J.; Sauer, M.; Stigloher, C.; Kleuser, B.; Seibel, J.; Schubert-Unkmeir, A. Click-Correlative Light and Electron Microscopy (Click-AT-CLEM) for Imaging and Tracking Azido-Functionalized Sphingolipids in Bacteria. *Sci. Rep.* **2021**, *11* (1), 4300.

(56) van Elsland, D. M.; Pujals, S.; Bakkum, T.; Bos, E.; Oikonomeas-Koppasis, N.; Berlin, I.; Neefjes, J.; Meijer, A. H.; Koster, A. J.; Albertazzi, L.; van Kasteren, S. I. Ultrastructural Imaging of Salmonella–Host Interactions Using Super-Resolution Correlative Light-Electron Microscopy of Bioorthogonal Pathogens. *ChemBioChem* **2018**, *19* (16), 1766–1770.

(57) Andrian, T.; Bakkum, T.; van Elsland, D. M.; Bos, E.; Koster, A. J.; Albertazzi, L.; van Kasteren, S. I.; Pujals, S. Super-Resolution Correlative Light-Electron Microscopy Using a Click-Chemistry Approach for Studying Intracellular Trafficking. In *Methods in Cell Biology*; Academic Press Inc., 2021; Vol. 162, pp 303–331.

(58) Nikić, I.; Estrada Girona, G.; Kang, J. H.; Paci, G.; Mikhaleva, S.; Koehler, C.; Shymanska, N. V.; Ventura Santos, C.; Spitz, D.; Lemke, E. A. Debugging Eukaryotic Genetic Code Expansion for Site-Specific Click-PAINT Super-Resolution Microscopy. *Angew. Chemie - Int. Ed.* **2016**, *55* (52), 16172–16176.

(59) Tuijtel, M. W.; Koster, A. J.; Jakobs, S.; Faas, F. G. A.; Sharp, T. H. Correlative Cryo Super-Resolution Light and Electron Microscopy on Mammalian Cells Using Fluorescent Proteins. *Sci. Rep.* **2019**, *9* (1), 1369.

(60) Moser, F.; Pražák, V.; Mordhorst, V.; Andrade, D. M.; Baker, L. A.; Hagen, C.; Grünewald, K.; Kaufmann, R. Cryo-SOFI Enabling Low-Dose Super-Resolution Correlative Light and Electron Cryo-Microscopy. *Proc. Natl. Acad. Sci.* **2019**, 201810690.

(61) Sun, D. en; Fan, X.; Shi, Y.; Zhang, H.; Huang, Z.; Cheng, B.; Tang, Q.; Li, W.; Zhu, Y.; Bai, J.; Liu, W.; Li, Y.; Wang, X.; Lei, X.; Chen, X. Click-ExM Enables Expansion Microscopy for All Biomolecules. *Nat. Methods* **2021**, *18* (1), 107–113.

(62) M'Saad, O.; Bewersdorf, J. Light Microscopy of Proteins in Their Ultrastructural Context. *Nat. Commun.* **2020**, *11* (1), 1–15.

(63) Li, N.; Lim, R. K. V; Edwardraja, S.; Lin, Q. Copper-Free Sonogashira Cross-Coupling for Functionalization of Alkyne-Encoded Proteins in Aqueous Medium and in Bacterial Cells. *J. Am. Chem. Soc.* **2011**, *133* (39), 15316–15319.

(64) Chenault, H. K.; Dahmer, J.; Whitesides, G. M. Kinetic Resolution of Unnatural and Rarely Occurring Amino Acids: Enantioselective Hydrolysis of N-Acyl Amino Acids Catalyzed by Acylase I. *J. Am. Chem. Soc.* **1989**, *111* (16), 6354–6364.

(65) Biagini, S. C. G.; Gibson, S. E.; Keen, S. P. Cross-Metathesis of Unsaturated Alpha-Amino Acid Derivatives. *J. Chem. Soc. Perkin Trans. 1* **1998**, *1*, 2485–2500.

(66) Dong, S.; Merkel, L.; Moroder, L.; Budisa, N. Convenient Syntheses of Homopropargylglycine. *J. Pept. Sci.* **2008**, *14* (10), 1148–1150.

(67) Albers, H. M. H. G.; Kuijl, C.; Bakker, J.; Hendrickx, L.; Wekker, S.; Farhou, N.; Liu, N.; Blasco-Moreno, B.; Scanu, T.; Den Hertog, J.; Celie, P.; Ovaa, H.; Neefjes, J. Integrating

Chemical and Genetic Silencing Strategies to Identify Host Kinase-Phosphatase Inhibitor Networks That Control Bacterial Infection. *ACS Chem. Biol.* **2014**, *9* (2), 414–422.

(68) Lutz, M. B.; Kukutsch, N.; Ogilvie, A. L. .; Rößner, S.; Koch, F.; Romani, N.; Schuler, G. An Advanced Culture Method for Generating Large Quantities of Highly Pure Dendritic Cells from Mouse Bone Marrow. *J. Immunol. Methods* **1999**, *223* (1), 77–92.

(69) Tokuyasu, K. T. A Technique for Ultracryotomy of Cell Suspensions and Tissues. *J. Cell Biol.* **1973**, *57* (2), 551–565.

(70) Peters, P. J.; Bos, E.; Griekspoor, A. Cryo-Immunogold Electron Microscopy. *Curr. Protoc. Cell Biol.* **2006**, *30* (1), 4.7.1-4.7.19.

(71) Schindelin, J.; Arganda-Carreras, I.; Frise, E.; Kaynig, V.; Longair, M.; Pietzsch, T.; Preibisch, S.; Rueden, C.; Saalfeld, S.; Schmid, B.; Tinevez, J. Y.; White, D. J.; Hartenstein, V.; Eliceiri, K.; Tomancak, P.; Cardona, A. Fiji: An Open-Source Platform for Biological-Image Analysis. *Nat. Methods* **2012**, *9* (7), 676–682.